Journal of Nuclear Medicine, published on February 22, 2019 as doi:10.2967/jnumed.118.223727

Molecular Imaging of the Glomerulus via Mesangial Cell Uptake of Radiolabeled Tilmanocept

Zhengtao Qin[1,2]
Carl K. Hoh[1,2]
Emilia S. Olson[1,2]
Amin Haghighat Jahromi[1,2]
David J. Hall[1,2]
Christopher V. Barback[1,2]
Young-Hyun You[3,4]
Mokoto Yanagita[5]
Kumar Sharma[3,4]
David R. Vera[1,2]

[1]Department of Radiology, University of California, San Diego, La Jolla California;
[2]UCSD In Vivo Cancer and Molecular Imaging Program;
[3]Center for Renal Translational Medicine, University of California, San Diego, La Jolla California;
[4]Department of Medicine, Division of Nephrology, University of California, San Diego, La Jolla, California;
[5]Department of Nephology, Kyoto University, Kyoto Japan

Address correspondence to D.R.V. (e-mail: dvera@ucsd.edu)

Section: Molecular Imaging

Running Title: Mesangial Cell Molecular Imaging

Key Words: Kidney Imaging, Tc-99m-tilmanocept, Ga-68-tilmanocept, mesangial cells

Word Count (title page, abstract, text, references, legends, and tables): 5,989

Abstract

An unmet need for the clinical management of chronic kidney disease is a predictive tool of kidney function during the first decade of the disease, when there is silent loss of glomerulus function. The objective of this study is to demonstrate receptor-mediated binding of tilmanocept to CD206 within the kidney, and provide evidence of kinetic sensitivity of this binding to renal function. **Methods:** Rats were positioned in a PET scanner with the liver and kidneys within the field of view. After an intravenous injection of ^{68}Ga-*IRDye800*-tilmanocept, using one of two scaled molar doses (0.02 nmol/g, n=5; or 0.10 nmol/g, n=5), or co-injection (n=3) of ^{68}Ga-*IRDye800*-tilmanocept (0.10 nmol/g) & unlabeled tilmanocept (5.0 nmol/g), or a negative control, ^{68}Ga-*IRDye800*-DTPA-galactosyl-dextran (0.02 nmol/g, n=5), each animal was imaged for 20 minutes followed by a wholebody scan. Frozen kidney sections were stained for podocytes and CD206 using immunofluorescence. Molecular imaging of diabetic *db*/*db* mice (4.9 wk, n=6; 7.3 wk, n=4; 13.3 wk, n=6) and non-diabetic *db*/*m* mice (n=6) was performed with fluorescent-labeled ^{99m}Tc-tilmanocept (18.5 MBq, 2.6 nmol). Thirty minutes after injection, blood, liver, kidneys, and urine were assayed for radioactivity. Renal time-activity curves were generated. **Results:** Rat PET wholebody images and time-activity curves of ^{68}Ga-*IRDye800*-tilmanocept demonstrated receptor-mediated renal accumulation with evidence of glomerular uptake. Activity within the renal cortex persisted during the 40-min study. Histologic examination demonstrated co-localization of CD206 and *IRDye800*-tilmanocept within the glomerulus. The glomerular accumulation of the co-injection and the negative control studies were significantly less than the CD206-targeted agent. The *db*/*db* mice displayed a multi-phasic renal time-activity curve with high urinary bladder accumulation; the non-diabetic mice exhibited renal uptake curves dominated by a single phase with low bladder accumulation. **Conclusion:** This study demonstrated receptor-mediated binding to the glomerular mesangial cells and kinetic sensitivity of tilmanocept to chronic renal disease. Given the role of mesangial cells during the progression of diabetic nephropathy, PET or SPECT renal imaging with radiolabeled tilmanocept may provide a non-invasive quantitative assessment of glomerular function.

Key Words: kidney imaging, ^{99m}Tc-tilmanocept, ^{68}Ga-tilmanocept, mesangial cells

INTRODUCTION

In 2017 the International Diabetes Federation estimated that the worldwide prevalence of diabetes would increase from 415 million persons in 2015 to 642 million in 2040 (*1*). Approximately 40% of persons with diabetes develop diabetic nephropathy as manifested by albuminuria and/or impaired glomerular filtration rate (*2*). As diabetic kidney disease progresses over 2-3 decades, it is critical to have a non-invasive measure which monitors early disease activity since markers such as albuminuria may often be transient and reductions in the estimates of glomerular filtration rate would already indicate more advanced disease (*3*). Consequently, the detection of renal dysfunction within the first decade of diabetic nephropathy is an unmet clinical need (*4*).

We propose external imaging of mesangial cell function as a biomarker for diabetic nephropathy. Our reasoning is based on the following. Mesangial cell matrix expansion is a histologic hallmark of diabetic nephropathy (*5*), which precedes the reduction of a patient's glomerulur filtration rate (*6*). Additionally, all of the clinical manifestations of diabetic nephropathy are highly correlated with mesangial matrix expansion (*7,8*). Lastly, there is evidence the mesangial expansion is reversable with therapy (*9*). There currently does not exist an imaging, serum, or urine biomarker that is sensitive to mesangial cell function (*10*).

We propose molecular imaging of mesangial cell function by targeting a radiopharmaceutical to CD206, which resides on the surface of mesangial cells (*11*). The imaging agent would be based on the design strategy for Tc-tilmanocept (*12*). ^{99m}Tc-tilmanocept, which has regulatory approvals in the U.S. and Europe for sentinel lymph node mapping, uses a DTPA-mannosyl-conjugate of dextran (Figure 1) and offers a number of advantages for the design of a renal imaging agent. The molecular weight of the dextran backbone can be adjusted to match the clinical requirements (*13*), and the number of receptor substrates per dextran can be altered to optimize receptor affinity (*14*). Tilmanocept can be labeled with ^{68}Ga for PET imaging (*15*). During the design process, dextran conjugates such as tilmanocept, can be labeled with a

fluorophore without the lose of receptor affinity (*16*). Additionally, chemical isomers of the receptor substrate can be used to produce a negative control with completely different receptor specificity, but similar hydrodymanic properties (Figure 1).

In this work, we present five independent experiments that demonstrate glomerular CD206 accumulation of tilmanocept and sensitivity to diabetic nephropathy. The first three experiments employed PET imaging of healthy rats to obtain adequate spatial resolution of renal cortex. We used a galactosyl-dextran conjugate, as a negative control. We used two different in vivo receptor saturation methods to demonstrate changes in renal PET time-activity data. We tested the histologic co-localization of fluorescent tilmanocept with a histoimmuno-fluorescent marker for CD206. Lastly, we tested the kinetic sensitivity to mesangial cell matrix expansion by comparing the renal time-activity curves of non-diabetic *db*/*m* and diabetic *db*/*db* mice, the latter animal model exhibits mesangial cell matrix expansion. We conclude with a discussion of the chemical modifications of tilmanocept that will optimize a molecular imaging protocol for staging a patient with early diabetic nephropathy.

MATERIALS AND METHODS

Reagents and Animals

Tilmanocept, diethylenetriaminepentaacetic acid (DTPA)-mannosyl-dextran and DTPA-dextran (*12*) were provided by Navidea Biopharmaceuticals (Dublin OH). *IRDye800CW*-NHS-ester was purchased for LI-COR Biosciences (Lincoln, NE) and *Cy5*-NHS-ester was purchased from GE Healthcare (Chicago IL). Female diabetic C57BLKS/J $LepR^{db}$/$LepR^{db}$ mice (*db*/*db*) and female non-diabetic C57BLKS/J $LepR^{db}$ (*db*/*m*) were purchased from Jackson Laboratories, (Bar Harbor ME). This study was approved by the UCSD IACUC.

Bimodal Radiopharmaceuticals

DTPA-galactosyl-dextran was synthesized (*12*) using cyanomethyl-2,3,4,6-tetra-*O*-acetyl-1-thio-ß-*D*-galactopyranoside (*17*). *IRDye800CW* or *Cy5* were covalently attached to tilmanocept or DTPA-galactosyl-dextran as previously described (*18*). The average fluorophore, chelator, carbohydrate, and amine densities for each dextran conjugate were measured by NMR (*18*) and was approximately 2 *IRDye800CW* or *Cy5* molecules, 5 DTPAs, 15 thioglycosides, and zero amino groups per dextran.

IRDye800-tilmanocept or *IRDye800*-DTPA-galactosyl-dextran were radiolabeled with ^{68}Ga, as previously described (*19*). *Cy5*-tilmanocept was radiolabeled with technetium-99m using tin reduction (*12*). Quality control of each fluorescent radiopharmaceutical was performed by instant thin layer chromatography (*19*). The radiochemical and optical purities of each injectate exceeded 96%.

PET Imaging of Healthy Rats: Demonstration of Glomerular CD206 Accumulation

PET Imaging of ^{68}Ga-labeled fluorescent-tilmanocept was performed using two scaled molar doses. Five rats (154 - 170 g) were injected with 0.02 nmol/g of ^{68}Ga-*IRDye800*-tilmanocept

(7.4 – 13.3 MBq) and five rats (171 - 214 g) were imaged (6.3 – 16.3 MBq) with a scaled molar dose of 0.10 nmol per gram of body weight. Additionally, five rats (221 - 252 g) were imaged with ^{68}Ga-*IRDye800*-galactosyl-dextran (0.02 nmol/g, 7.0 – 13.3 MBq), and three rats (166 - 180 g) were imaged after a co-injection of ^{68}Ga-*IRDye800*-tilmanocept (0.1 nmol/g, 5.8 – 4.7 MBq) and unlabeled tilmanocept (5.0 nmol/g). After positioning both kidneys are within the field-of-view of a high-resolution PET scanner (*Vista DR*, G.E. Healthcare), a 20-minute dynamic scan was performed and immediately followed with by wholebody imaging study. At 40 minutes post injection, each rat was euthanized by CO_2 affixation. Both kidneys, the entire liver, and urinary bladder were excised, rinsed, weighed, assayed for radioactivity (*Gamma 8000*, Beckman Instruments, Fullerton CA, 500 – 600 keV), bisected, placed in embedding medium, and stored at -80 ^{o}C.

The dynamic scan was reconstructed into cross-sections with 30-second time intervals. Ten contiguous coronal cross-sections from each kidney and liver were used to generate decay-corrected time-activity curves. These curves were scaled to percent-of-injected dose per gram based on measurements of each kidney and liver obtained at 40 min post-injection. The wholebody images were reconstructed into trans-axial cross-sections and reformatted into maximum intensity projection (MIP) images (*20*).

Immunohistochemistry: Demonstration of CD206 Targeting

The bisected rat kidneys were cut into contiguous 5-micron cryostat sections, stored at -80 ºC, and dried at room temperature before immunofluorescent staining. All incubation solutions contained 40 mM divalent cations. After fixation, the slides were washed and incubated in PBS containging 0.5% Triton X-100. This was followed by incubation in PBS containing 1% BSA and 0.02% Triton X-100. The two primary antibodies: anti-mannose receptor antibody (ab-64693, ABCAM, Cambridge, MA) and anti-podocyte antibody (sc-22296, Santa Cruz Biotechnology, Dallas, TX) were incubated overnight at 4 ºC. After as similar incubation with the secondary

antibodies bearing *Alexa Fluor 488 or Alexa Fluor 647*, the slides were washed, dried, mounted, and stored in dark at -20°C.

The histologic sections were examined under a fluorescence microscope (Nikon E600). Three filter sets were used: (Ex=470 nm, Em=525 nm), which represented the podocyte stain; (Ex=620 nm, Em=700 nm), which represented the CD206 stain; (Ex=747 nm, Em=776 nm) for *IRDye800*-tilmanocept or *IRDye800*-DTPA-galactosyl-dextran.

Gamma Imaging of Mice: Demonstration of Sensitivity to Chronic Renal Disease

Male diabetic *db*/*db* mice were imaged at 4.9 (n=6), 7.3 (n=5), and 13.3 (n=6) weeks of age. Additionally, 4.1 week-old male non-diabetic *db*/*m* mice (n=6) were imaged. After weighing, each animal was anesthetized (2% isoflurane, 200 ml/min O_2), positioned (ventral view) atop a high-resolution gamma imager (γ *Imager*, BioSpace, Paris, France) fitted with a high-resolution low energy collimator. After a 25-minute dynamic imaging study (^{99m}Tc -labeled *Cy5*-tilmanocept, ~18.5 MBq, 2.6 nmol), both kidneys and the urinary bladder were excised, weighed, and assayed for radioactivity (100 – 200 keV) with a known dilution of the injectate. Regions-of-interests (ROIs) were drawn around a portion of the left kidney. Decay-corrected time-activity curves were generated and normalized to the percent-of-injected dose per gram.

Statistical Analysis

We used the Student-t test (JMP, version 9, 2010, SAS Institute, Cary NC) to calculate a two-tailed test of statistical significance assuming equal variances. We considered a two-sided *P*-value of less than 0.05 to be statistically significant.

RESULTS

PET Imaging of Healthy Rats: Demonstration of Glomerular CD206 Accumulation

The biodistribution studies of the CD206-specific molecule *IRDye800*-tilmanocept and the negative control, *IRDye800*-DPTA-galactosyl-dextran, demonstrated receptor-mediated binding of tilmanocept within the kidney. Figure 2 summarizes these studies graphically. The low scaled molar dose studies demonstrated a statistically significant ($P < 0.001$) difference in renal uptake (red bars) between tilmanocept and ^{68}Ga-*IRDye800*-DTPA-galactosyl-dextran (FL-*gal*-Dextran). The liver accumulation (green bars) at 40 minutes post-injection of the low dose (0.02 nmol/g) tilmanocept and ^{68}Ga-*IRDye800*-DTPA-galactosyl-dextran doses (FL-*gal*-Dextran, 0.02 nmol/g) were significantly ($P < 0.001$) higher than the hepatic accumulation (2.94 ±0.67 nmol/g) of the high dose (0.10 nmol/g) FL-tilmanocept studies. Saturation of the hepatic CD206 permitted more fluorescent-tilmanocept to reach the kidneys. The percent-of-injected dose of urinary bladder and urine was significantly ($P = 0.042$) higher for the low-dose fluorescent-tilmanocept studies (14.2 ±7.8 %), compared to the low-dose fluorescent-galactosyl-dextran studies (5.57 ±1.81 %). Neither of the low-dose studies exhibited a statistically different urinary bladder accumulation compared to the high dose tilmanocept (8.16 ±4.42 %).

PET dynamic imaging demonstrated receptor-mediated renal accumulation by ^{68}Ga-*IRDye800*-tilmanocept. Four examples of renal time-activity curves are displayed in Figure 3. Renal accumulation by a high scaled molar dose (FL-tilmanocept, green) of ^{68}Ga-fluorescent-tilmanocept exhibited a longer time to peak (8.8 min) and higher accumulation than an imaging study that used a low scaled molar dose (FL-tilmanocept, red) of fluorescent-tilmanocept. The liver accumulation for the same high scaled molar dose (S.I. Fig. 1, FL-tilmanocept, green) studies exhibited a nearly flat curve with a very low peak value (31 %). This permitted the kidneys to bind a greater fraction of the injectate. A negative control study (FL-gal-Dextran, yellow) exhibited negligible renal accumulation and high (81 %ID) liver uptake (S.I. Fig. 1, yellow); the highest kidney values occurred early post-injection (~3.2 min) and most probably were produced by activity within the renal blood pool. A co-

injection (“blocking”) study (Fig. 3, blue) exhibited low renal accumulation, which plateaued (~ 7.5 %/g) within 3 minutes of injection. The liver time-activity curve from this study also exhibited saturated binding (S.I. Fig. 1, blue). The shape of the kidney “blocking” curves differed significantly from the “non-blocked” 0.10-nmol/g injections (green) that did not contain a 5.0-nmol/g blocking dose of cold tilmanocept. The “non-blocked” curves (green) exhibited a sustanded renal accumulation for 10 minutes and achieved a percent-of-injected dose per gram within each kidney that was double the plateau value of the “blocked” dose” (blue).

PET imaging demonstrated receptor-mediated accumulation of ^{68}Ga-*IRDye800*-tilmanocept in the renal cortex. Figure 4A, is a ventral projection wholebody MIP imaging (20 – 40 min PI) and is representative of a high molar dose (0.1 nmol/g) ^{68}Ga-labeled-fluorescent-tilmanocept study, which exhibited diminished liver accumulation (3.1 %/g, green arrow) compared to the kidneys (12 %ID/g red arrow); the urinary bladder (yellow arrow) accumulated 14 % of the injected dose. A PET MIP wholebody image (Fig 4B) from a low molar dose (0.02 nmol/g) study demonstrated a higher liver accumulation (5.6 %/g, green arrow) than the high scaled dose study. The kidneys accumulated 9.2 %/g (Fig 4B, red arrow); the urinary bladder (yellow arrow) accumulated 8.3 % of the dose. The renal images of all ten ^{68}Ga-fluorescent-tilmanocept studies exhibited increased activity at the rim of the cortex. Figure 4C (the sum of 10 contiguous coronal cross-sections) clearly delineates activity within the renal cortex. Activity in the right and left cortex (red arrows) dominate the renal image. The green arrows mark the dorsal aspect of the right and left lobes of the liver. A negative control study (Fig 4D, MIP, wholebody, 20 – 40 min PI) using ^{68}Ga-*IRDye800*-galactosyl-dextran (0.02 nmol/g) exhibited significantly less radioactivity in the kidneys (3.1 %/g, red arrow).

Immunohistochemistry: Demonstration of CD206 Targeting

Histomicrographs of all ten rat kidneys from the high dose ^{68}Ga-*IRDye800*-tilmancoept studies demonstrated tilmanocept binding to the CD206 receptor within the glomerulus. Figure 5 displays four histomicrographs from the same section using 60x magnification. Figure 5A is a single-channel

(*AlexaFluor647*) demonstrating the distribution of CD206 (green). Figure 5B is a single-channel (*IRDye800CW*, 60x) composite representing the distribution of *IRDye800*-tilmanocept (red). Figure 5C is a two-channel (*AlexaFluor488*, *IRDye800CW*) overlay composite, which demonstrates CD206 (green) distribution within the glomerular compartment defined by podocytes stained with *Alexa-488* (grey). Lastly, Figure 5D is another two-channel (*AlexaFluor647, IRDye800CW*) overlay composite that demonstrates tilmanocept (red) and CD206 (green) co-localization (yellow) within one glomerulus.

Histomicrographs from the negative control studies demonstrated the specificity of tilmanocept for mesangial CD206 (Supplementary Figure 2). Histomicrographs from healthy rat kidneys excised 40 minutes after injection of ^{68}Ga-*IRDye800*-DTPA-galactosyl-dextran exhibited a very low presence of *IRDye800*. Histomicrographs using 20x magnification (Supplementary Figure 3) also demonstrated co-localization of tilmanocept and CD206. These wider-field views displayed extra-golumerular regions of *IRDye800* (red) which are consistent with filtered *IRDye800*-tilmanocept within the renal tubules.

Gamma Imaging of Mice: Demonstration of Sensitivity to Chronic Renal Disease

Dynamic imaging of *db*/*m* and *db*/*db* mice demonstrated kinetic sensitivity to chronic kidney disease. These experiments are summarized in Figure 6. The average time (blue bars) at which the non-diabetic *db*/*m* renal curves peaked was significantly ($P < 0.005$) longer than the average time-to-peak value of the curves from the 4.9 week-old *db*/*db* diabetic mice, the 7.3 week-old *db*/*db* mice, and the curves from the 13.3 week-old *db*/*db* mice. The renal %ID/g (red bars) of ^{99m}Tc-labeled *Cy5*-tilmanocept by non-diabetic *db*/*m* mice far exceeded the renal accumulation of the diabetic *db*/*db* mice at all three ages. The percent-of-injected dose in the urine (yellow bars) of the *db*/*m* mice was which was significantly lower ($P < 0.03$) than all age groups of the *db*/*db* mice.

Figure 7A displays representative ^{99m}Tc-labeled *Cy5*-tilmanocept scaled time-activity curves from the left kidneys of diabetic and non-diabetic mice. The four curves illustrate the profound difference in shape between the time-activity curves of the non-diabetic and three diabetic mice. The non-diabetic *db*/*m* mouse (blue diamonds) exhibited a renal uptake curve dominated by a single phase during the 25-minute dynamic imaging study. The left kidney curve of the non-diabetic mouse peaked 22 minutes after injection at 5.5 % of the injected dose (blue diamonds). The urinary bladder with contents of the non-diabetic *db*/*m* mice at 30 minutes post-injection contained 1.1 percent of the dose. Figure 7B is an expanded view of Fig 7A which demonstrates increased renal accumulation of tilmanocept with increasing age. The curves from the 4.9-, 7.3-, and 13.3-week-old diabetic kidneys peaked at 4.0 % (at 2.5 min, green curve), 4.4 % (at 2.0 min, yellow curve), and 4.9 % at 1.8 minutes (red curve), respectively.

DISCUSSION

PET Imaging of Healthy Rat: Demonstration of Glomerular CD206 Accumulation

This work provided *in vivo* demonstration that CD206 is the molecular target when imaging the kidney with radiolabeled tilmanocept. We demonstrated a statistically significant loss of renal accumulation by the galactosyl-conjugate of dextran (*21*), which binds to the asialoglycoprotein receptor in the liver and does not bind to CD206 in the kidney. Using time-activity curves at two different scaled molar doses, we demonstrated that the renal accumulation of ^{68}Ga-labeled fluorescent-tilmanocept can be saturated; which is the hallmark of a receptor-mediated process (*22*). The standard method for demonstrating receptor-specific binding (*23*), a "receptor blocking" study, substantually dimimished the renal accumulation of ^{68}Ga-labeled tilmanocept.

Immunohistochemistry: Demonstration of CD206 Targeting

We demonstrated the histologic co-localization of *IRDye800*-tilmanocept with a fluorescent marker for CD206. A substaintal majority of the *IRDye800CW* fluorescence was localized within the confines of the glomerulus, as defined by podocyte staining. .

Gamma Imaging of Mice: Demonstration of Sensitivity to Chronic Renal Disease

The *db*/*db* and *db*/*m* mice imaging studies (Figs 6. and 7.) demonstrated kinetic sensitivity of tilmanocept to renal function in chronic renal disease. The *db*/*db* mouse (*24,25*) is a rodent model of of genetic diabetes, which mirrors the progression of glomerular changes found in human diabetes (*4,26*). At 8 weeks of age, diabetic *db*/*db* mice have the same serum creatinine levels and same mesangial matrix fraction as non-diabetic *db*/*m* mice of the same age (*27*). At 12 and 16 weeks of age the mesangial matrix fraction of *db*/*db* mice expands 2- and 3.5-fold, respectively. This expansion was statistically significant when compared to the *db*/*db* mice at 4 weeks and the *db*/*m* mice of the same age (*27*). The elevated ^{99m}Tc-tilmanocept renal and urine accumulation (Fig 6.) of the diabetic mice is consistant with hyperfiltration observed by *db*/*db* mice and human diabetic nephopathy (*26*).

The Mesangial Cell as an Alternative Molecular Imaging Target

Intra-glomerular mesangial cells offer a new cellular target for molecular imaging of the kidney. After delivery to the kidney by renal plasma flow (Fig 8, arrow 1) an imaging agent, can be passively ultra-filtered into the proximal tubule depending on its size and charge (Fig 8, insert A, arrow 2) or extracted from the plasma by the mesangial cells (Fig 8, insert A, arrow 3). Both routes require the passage through a highly porous and negatively charged (*28*) fenestrated capillary endothelium (Fig 8, insert B). Molecules that are passively filtered into Bowman's capsule transverse a dense network of glycoprotein and collagen known as the glomerular basement membrane (GBM) (Fig 8, insert B), which is also negatively charged (*29*) followed by a negatively charged slit diaphragm between the podocytes. Molecules that approach the mesangial cells must transverse a fibrillary matrix (Fig 8, insert A, arrow 3), also known as the mesangial cell matrix.

An important physiologic function of mesangial cells is thier active participation in the formation and maintenance of the mesangial cell matrix, and the GBM (*30*). Thickening of the GBM and expansion of the mesangium are the major lesions of diabetic nephropathy leading to renal dysfunction in diabetes patients (*31*). These lesions occur early in the progression of the disease. Both the cellular and matrix components of the mesangium increase in relative volume during diabetes (*32*), with a 57% increase in cellular volume and 185 % increase in matrix volume. Other significant mesangial cell functions are the regulation of glomerular plasma flow, by their smooth muscle properties; the immunologic recognition and clearance of cellular "debris" within the mesangium; and the monitoring of mesangial glucose concentration.

Clinical Significance

Tilmanocept may offer a non-invasive alternative to renal biopsy for diagnosis of early glomerular disease. Many potential drug targets have emerged from this research including the vasopressin V1α receptor (*33*), the NF-κB receptor (*34*) and $\alpha_V\beta_3$ (*35*). Agents that target these receptors are most effective during the early phases of inflammation, where they block the inflammatory response that

leads to fibrosis. This strategy necessitates early recognition of disease. This has led to calls for universal renal biopsies in newly diagnosed diabetic patients to identify early treatable disease (*36*). Percutaneous biopsy is invasive and the procedure alone carries a 7-10% risk of minor complication such as bleeding or pain and a 0.1-0.5 % risk of a major complication requiring a nephrectomy or iatrogenic arteriovenous malformation (*37*). Given 1.7 million new cases of Type II diabetes in 2012 (*38*), this would lead to 119,000 - 170,000 patients with bleeding and pain following biopsy, and 1,700 to 7,500 patients with major complications such as arteriovenous fistula or bleeding requiring partial nephrectomy (*37*). Finally, biopsy suffers from under-sampling, as only 10 out of 617,000 glomeruli per kidney are actually evaluated in the course of a renal biopsy (*39*).

Optimization of the Molecular Imaging Agent

Our next step toward the development of radiolabeled tilmanocept as a renal molecular imaging agent will be the design of a protocol that matches the clinical setting. Knowing that the cellular target within the kidney is responsible for mesangial matrix expansion, our design strategy will maximize the sensitivity of tilmanocept imaging to changes in both mesangial matrix permeability (Fig 8, inset A, arrow 3), and receptor density. The following chemical features would make CD206-targeted molecular imaging highly sensitive to tilmanocept mesangial matrix permeability and receptor density: 1) a molar dose of tilmanocept that does not saturate the receptor sites in healthy kidneys, 2) a neutral charge distribution of the molecular imaging agent, and 3) an imaging agent of moderately high molecular diameter. The latter property will be used to eliminate ultra-filtration through the Bowman's capsule, which will increase mesangial cell accumulation. A CD206-specific dextran with a molecular radius equal to albumin will not be filtered by the GBM, but will still retain easy access through the mesangial matrix. The rat golmerulus has been studied by electron microscopy (*40,41*) revealing an average mesangial matrx pore size that is ten-fold larger than that of the GBM.

Our design hypothesis is that early mesangial matrix expansion will increase the permeability of tilmanocept through the mesangial matrix, which in turn will increase delivery of the molecular

imaging agent to mesangial cells. This is consistent with the series of time-activity curves (Fig 7A.) from diabetic mice, where early time-points displayed (Fig 7B.) fast renal accumulation with increasing age. This hypothesis is based on measurements of collagen VI density, which decreases during mesangial matrix expansion (*42*). The increased delivery to the mesangial cell surface will expose more tilmanocept to the limited number of CD206 receptors. The result will be a time-activity curve with a different shape than a curve from a healthy kidney. The green curve in Figure 3 provides an example. This study used a high scaled molar dose, which produced a curve that exhibits receptor saturation distinguished by a slower and linear portion of the curve (5 – 10 minutes post injection) as it approaches it's peak value.

For routine clinical applications, technetium-99m is the nuclide of choice. The typical imaging protocol could consist of a 100 MBq dose of ^{99m}Tc-tilmanocept administered intravenously followed by a 20-minute dynamic imaging study; the patient would lie supine with both kidneys within the field-of-view of an anterior-facing camera head with the second camera head acquiring a posterior view. The dynamic study would provide a quantitative basis to assess the glomerular function of each kidney.

Clinical research could utilize PET/MRI or PET/CT with gallium-68. PET imaging with motion-correction via simultaneous MRI acquisition, could provide regional estimates of mesangial cell function. Although it has been demonstrated (*5*) that mesangial expansion is characterized by a 3-fold increase in mesangial matrix over mesangial cell volume, dynamic PET/MRI using higher scaled molar doses of ^{68}Ga-tilmanocept could provide independent measurements of permeability-surface area of the mesangial matrix, as well as receptor density. The latter measurement should be directly proportional to mesangial cell density. An example of this approach is hepatocellular imaging of ^{99m}Tc-galactosyl-neoglycoalbumin (*43,44*), where kinetic modeling demonstrated a linear relationship between receptor amount and viable hepatocellular mass within the entire liver (*44*).

Imaging of specific molecular targets, such as CD206 within the glomerulus and the organic anion transporter 1 of proximal tubules (*45,46*), represent complementary strategies for the non-invasive

measurement of renal function. Both targets are energy-dependent transporters of physiologically significant molecules at two critical cell types that serve different functions within the kidney. Radiopharmaceuticals ^{99m}Tc-DTPA and ^{99m}Tc-MAG3 have specific roles, but are not accepted (*47*) as the primary indication for glomerular filtration rate or renal blood flow. Most importantly, the detection of blood flow, filtration, and structural abnormalities, such as cortical atrophy and tumors, are unable to detect the early stages of chronic kidney disease, such as diabetes, or immune complex diseases, such as lupus or IgA nephropathy. Currently, there are no biomarker for the early detection of diabetic nephropathy (*48*) and immune complex diseases of the kidney (*49*). Consequently, these diseases are screened by GFR estimates from serum creatinine measurments and urine micro-albumin concentrations (*50*), both of which are insensitive in the first decade of type 1 and type 2 diabetes (*31,51,52*).

CONCLUSION

This study demonstrated receptor-mediated binding to the glomerular mesangial cells and kinetic sensitivity of tilmanocept to chronic renal disease. Given the early role of mesangial cells during the progression of chronic kidney disease, PET or SPECT renal imaging of CD206 may provide a non-invasive and highly sensitive quantitative assessment of glomerular function based upon specific physiologic and cellular components that are central to the healthy kidney. A SPECT/CT or PET/CT protocol that accurately staged early diabetic kidney disease may help to establish a precise baseline for frequent surveillance by a serum or urine biomarker.

DISCLOSURE

David Vera is the inventor of tilmanocept. The remaining authors disclose no potential conflicts of interest relevant to this article.

ACKNOWLEDGMENTS

The authors thank Dr William C. Eckelman and Dr Sushrut Waikar for their helpful discussions. We also thank the staffs of the In Vivo Imaging Shared Resource and the Microscope Shared Resource at the UCSD Moores Cancer Center. This work was funded in part by the NCI In Vivo Cancer and Molecular Imaging Program (P50 CA128346). Dr Jahromi was supported by NIH T32-4T32EB005970. This work was presented to the NIDDK Renal Imaging Workshop, July 12-13, 2018, Bethesda MD; the authors wish to acknowledge the many helpful comments from the workshop participants.

REFERENCES

1. Ogurtsova K, da Rocha Fernandes JD, Huang Y, et al. IDF Diabetes Atlas: Global estimates for the prevalence of diabetes for 2015 and 2040. *Diabetes Res Clin Pract.* 2017;128:40-50.
2. KDOQI. KDOQI clinical practice guidelines and clinical practice recommendation for diabetes and chronic kidney disease. *Am J Kidney Dis.* 2007;49:S12-S1544.
3. Alicic RZ, Rooney MT, Tuttle KR. Diabetic Kidney Disease: Challenges, Progress, and Possibilities. *Clin J Am Soc Nephrol.* 2017;12:2032-2045.
4. Thomas MC, Brownlee M, Susztak K, et al. Diabetic kidney disease. *Nat Rev Dis Primers.* 2015;1:15018.
5. Steffes MW, Osterby R, Chavers B, Mauer SM. Mesangial expansion as a central mechanism for loss of kidney function in diabetic patients. *Diabetes.* 1989;38:1077-1081.
6. Katz A, Caramori ML, Sisson-Ross S, Groppoli T, Basgen JM, Mauer M. An increase in the cell component of the cortical interstitium antedates interstitial fibrosis in type 1 diabetic patients. *Kidney Int.* 2002;61:2058-2066.
7. Mauer SM, Steffes MW, Ellis EN, Sutherland DE, Brown DM, Goetz FC. Structural-functional relationships in diabetic nephropathy. *J Clin Invest.* 1984;74:1143-1155.
8. Caramori ML, Kim Y, Huang C, et al. Cellular basis of diabetic nephropathy: 1. Study design and renal structural-functional relationships in patients with long-standing type 1 diabetes. *Diabetes.* 2002;51:506-513.
9. Fioretto P, Steffes MW, Sutherland DE, Goetz FC, Mauer M. Reversal of lesions of diabetic nephropathy after pancreas transplantation. *N Engl J Med.* 1998;339:69-75.
10. Sabbisetti V, Bonventre JV. Biomarkers in acute and chronic kidney diseases. In: Tall MW, Chertow GM, Marsden PA, Skorecki K, Yu ASL, Brenner BM, ed. Brenner & Rector's the Kidney. ninth ed. Philadelphia: Elsevier Saunders, 2012: 1016-1042. vol 1).
11. Linehan SA, Martinez-Pomares L, Stahl PD, Gordon S. Mannose receptor and its putative ligands in normal murine lymphoid and nonlymphoid organs: In situ expression of mannose

receptor by selected macrophages, endothelial cells, perivascular microglia, and mesangial cells, but not dendritic cells. *J Exp Med.* 1999;189:1961-1972.

12. Vera DR, Wallace AM, Hoh CK, Mattrey RF. A synthetic macromolecule for sentinel node detection: (99m)Tc-DTPA-mannosyl-dextran. *J Nucl Med.* 2001;42:951-959.
13. Sirlin CB, Vera DR, Corbeil JA, Caballero MB, Buxton RB, Mattrey RF. Gadolinium-DTPA-dextran: a macromolecular MR blood pool contrast agent. *Acad Radiol.* 2004;11:1361-1369.
14. Vera DR, Krohn KA, Stadalnik RC, Scheibe PO. Tc-99m galactosyl-neoglycoalbumin: in vitro characterization of receptor-mediated binding. *J Nucl Med.* 1984;25:779-787.
15. Stroup SP, Kane CJ, Farchshchi-Heydari S, et al. Preoperative sentinel lymph node mapping of the prostate using PET/CT fusion imaging and Ga-68-labeled tilmanocept in a dog model. *Clin Exp Metastasis.* 2012;29:673-680.
16. Emerson DA, Limmer KK, Hall DJ, et al. A receptor-targeted fluorescent radiopharmaceutical for multi-reporter sentinel lymph node imaging. *Radiology.* 2012;265:186-193.
17. Vera DR, Stadalnik RC, Krohn KA. [Tc-99m]galactosyl-neoglycoalbumin: preparation and preclinical studies. *J Nucl Med.* 1985;26:1157-1167.
18. Qin Z, Hall DJ, Liss MA, et al. Optimization via specific fluorescence brightness of a receptor-targeted probe for optical imaging and positron emission tomography of sentinel lymph nodes. *J Biomed Opt.* 2013;18:101315.
19. Qin Z, Hoh CK, Hall DJ, Liss MA, Kane CJ, Vera DR. Radiolabeling and Quality Control of fluorescent-labeled tilmanocept for tri-model sentinel lymph node mapping. *Nucl Med Biol.* 2015;42:917-922.
20. Wallis JW, Miller TR. Three-dimensional display in nuclear medicine and radiology. *J Nucl Med.* 1991;32:534-546.
21. Vera DR, Hall DJ, Hoh C, Gallant P, McIntosh L, Mattrey R. Cy5.5-DTPA-galactosyl-dextran: A fluorescent probe for in vivo measurement of receptor biochemistry. *Nucl Med Biol.* 2005;32:687-693.

22. Vera DR, Krohn KA, Stadalnik RC, Scheibe PO. [Tc-99m]galactosyl-neoglycoalbumin: in vivo characterization of receptor-mediated binding to hepatocytes. *Radiology.* 1984;151:191-196.

23. Eckelman WC, Frank JA, Brechbiel M. Theory and practice of imaging saturable binding sites. *Invest Radiol.* 2002;37:101-106.

24. Hummel KP, Dickie MM, Coleman DL. Diabetes, a new mutation in the mouse. *Science.* 1966;153:1127-1128.

25. Cohen MP, Clements RS, Hud E, Cohen JA, Ziyadeh FN. Evolution of renal function abnormalities in the db/db mouse that parallels the development of human diabetic nephropathy. *Exp Nephrol.* 1996;4:166-171.

26. Sharma K, McCue P, Dunn SR. Diabetic kidney disease in the db/db mouse. *Am J Physiol Renal Physiol.* 2003;284:F1138-1144.

27. Cohen MP, Lautenslager GT, Shearman CW. Increased urinary type IV collagen marks the development of glomerular pathology in diabetic d/db mice. *Metabolism.* 2001;50:1435-1440.

28. Sorensson J, Bjornson A, Ohlson M, Ballermann BJ, Haraldsson B. Synthesis of sulfated proteoglycans by bovine glomerular endothelial cells in culture. *Am J Physiol Renal Physiol.* 2003;284:F373-380.

29. Kanwar YS, Farquhar MG. Presence of heparan sulfate in the glomerular basement membrane. *Proc Natl Acad Sci U S A.* 1979;76:1303-1307.

30. Schlondorff D. The glomerular mesangial cell: an expanding role for a specialized pericyte. *FASEB J.* 1987;1:272-281.

31. Parving H-H, Mauer M, Fiorette P, Rossing P, E R. Diabetic Nephropathy. In: Tall MW, Chertow GM, Marsden PA, Skorecki K, Yu ASL, Brenner BM, ed. Brenner & Rector's the Kidney. ninth ed. Philadelphia: Elsevier Sanders, 2012: 1417. vol 1).

32. Steffes MW, Bilous RW, Sutherland DE, Mauer SM. Cell and matrix components of the glomerular mesangium in type I diabetes. *Diabetes.* 1992;41:679-684.

33. Windt WA, Tahara A, Kluppel AC, de Zeeuw D, Henning RH, van Dokkum RP. Early, but not late therapy with a vasopressin V1a-antagonist ameliorates the development of renal damage after 5/6 nephrectomy. *J Renin Angiotensin Aldosterone Syst.* 2006;7:217-224.

34. Oguiza A, Recio C, Lazaro I, et al. Peptide-based inhibition of IkappaB kinase/nuclear factor-kappaB pathway protects against diabetes-associated nephropathy and atherosclerosis in a mouse model of type 1 diabetes. *Diabetologia.* 2015;58:1656-1667.

35. Maile LA, Busby WH, Gollahon KA, et al. Blocking ligand occupancy of the alphaVbeta3 integrin inhibits the development of nephropathy in diabetic pigs. *Endocrinology.* 2014;155:4665-4675.

36. Gonzalez Suarez ML, Thomas DB, Barisoni L, Fornoni A. Diabetic nephropathy: Is it time yet for routine kidney biopsy? *World J Diabetes.* 2013;4:245-255.

37. Brachemi S, Bollee G. Renal biopsy practice: What is the gold standard? *World J Nephrol.* 2014;3:287-294.

38. Centers for Disease Control and Prevention. Estimates of Diabetes and Its Burden in the United States, 2014. In: Atlanta, GA: National Center for Chronic Disease Prevention and Health Promotion, 2014:

39. Nyengaard JR, Bendtsen TF. Glomerular number and size in relation to age, kidney weight, and body surface in normal man. *Anat Rec.* 1992;232:194-201.

40. Latta H, Fligiel S. Mesangial fenestrations, sieving, filtration, and flow. *Lab Invest.* 1985;52:591-598.

41. Takami H, Naramoto A, Nakazawa K, Shigematsu H, Ohno S. Ultrastructure of glomerular mesangial matrix by quick-freeze and deep-etch methods. *Kidney Int.* 1990;38:1211-1215.

42. Moriya T, Groppoli TJ, Kim Y, Mauer M. Quantitative immunoelectron microscopy of type VI collagen in glomeruli in type I diabetic patients. *Kidney Int.* 2001;59:317-323.

43. Stadalnik RC, Kudo M, Eckelman WC, Vera DR. In vivo functional imaging using receptor-binding radiopharmaceuticals: Technetium-99m-galactosyl-neoglycoalbumin as a model. *Invest Radiol.* 1993;28:64-70.

44. Miki K, Kubota K, Inoue T, Vera DR, Makuuchi M. Receptor measurements via TcGSA kinetic modeling are proportional to functional hepatocellular mass. *J Nucl Med.* 2001;42:733-737.

45. Lipowska M, Klenc J, Jarkas N, Marzilli LG, Taylor AT. Monoanionic (99m)Tc-tricarbonyl-aminopolycarboxylate complexes with uncharged pendant groups: Radiosynthesis and evaluation as potential renal tubular tracers. *Nucl Med Biol.* 2017;47:48-55.

46. Lipowska M, Jarkas N, Voll RJ, et al. Re(CO)3([(18)F]FEDA), a novel (18)F PET renal tracer: Radiosynthesis and preclinical evaluation. *Nucl Med Biol.* 2018;58:42-50.

47. Blaufox MD. Renal background correction and measurement of split renal function: The challenge : Editorial Comment: EJNM-D-15-00322, M Donald Blaufox, MD, PhD. *Eur J Nucl Med Mol Imaging.* 2016;43:548-549.

48. Currie G, McKay G, Delles C. Biomarkers in diabetic nephropathy: Present and future. *World J Diabetes.* 2014;5:763-776.

49. De Vriese AS, Fervenza FC. Con: Biomarkers in glomerular diseases: putting the cart before the wheel? *Nephrol Dial Transplant.* 2015;30:885-890.

50. Snyder S, Pendergraph B. Detection and evaluation of chronic kidney disease. *Am Fam Physician.* 2005;72:1723-1732.

51. McGowan T, McCue P, Sharma K. Diabetic nephropathy. *Clin Lab Med.* 2001;21:111-146.

52. Saito R, Rocanin-Arjo A, You YH, et al. Systems biology analysis reveals role of MDM2 in diabetic nephropathy. *JCI Insight.* 2016;1:e87877.

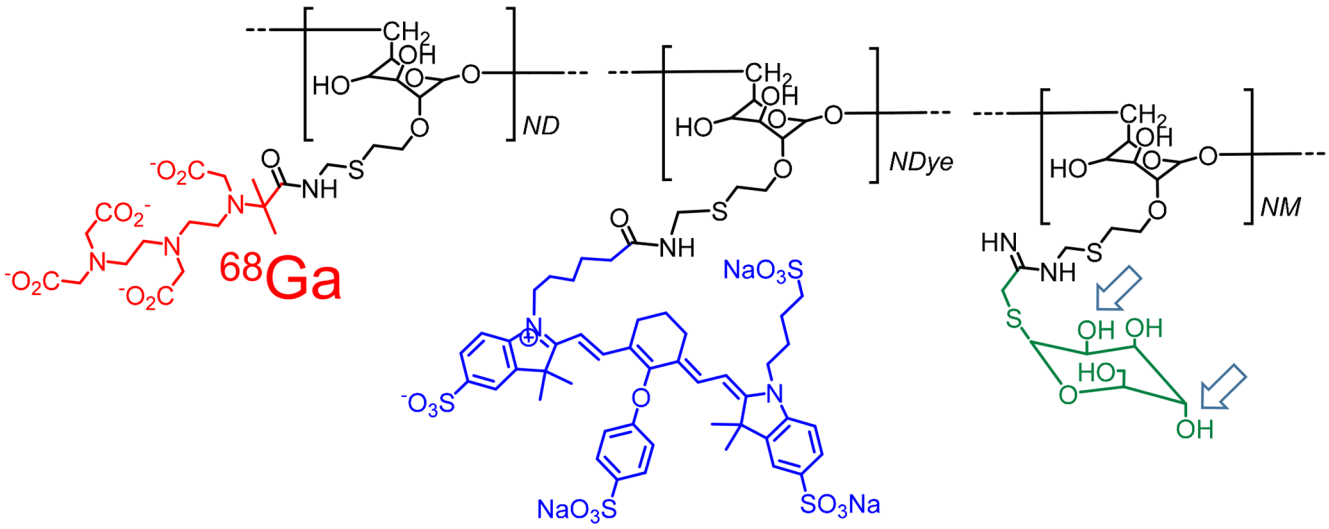

Figure 1: The bimodal molecular imaging agent, ^{68}Ga-labeled *IRDye800*-tilmanocept, consists of a modified dextran backbone (black), which carries the CD206 receptor substrate, mannose (green); a metal chelator, DTPA (red); and the fluorescent tag, *IRDye800CW* (blue). Isomeric change of the hydroxyls at the C2 and C4 carbons of the receptor substrate (arrows) produces a glycoconjugate that binds only to the asialoglycoprotein receptor, which is specific to hepatocytes.

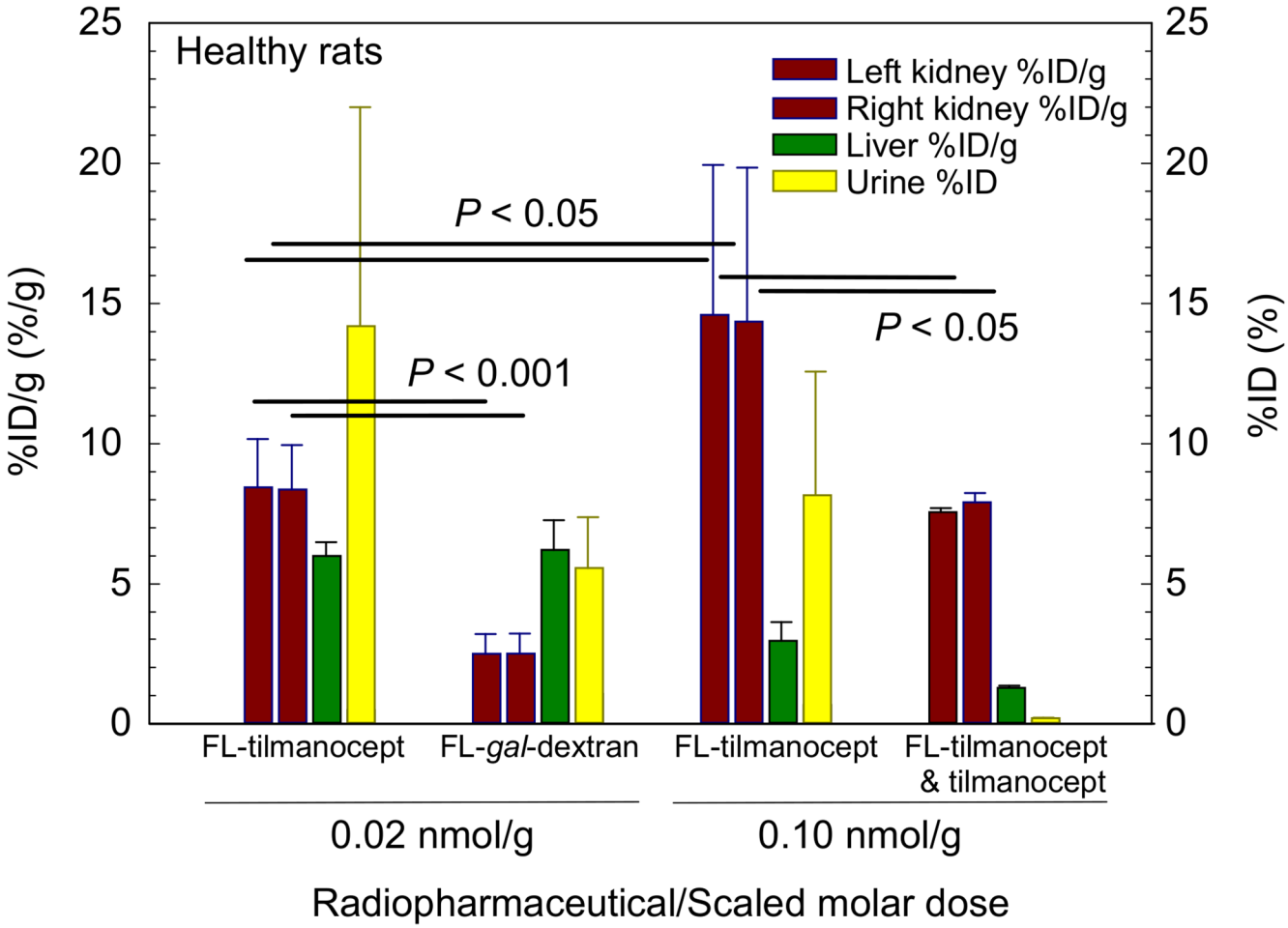

Figure 2: The in vivo demonstration of receptor-mediated binding by tilmanocept. Kidneys, liver, and urine were harvested 40 minutes after inject of: a low scaled molar dose of ^{68}Ga-labeled-*IRDye800*-tilmanocept (FL-tilmanocept),or ^{68}Ga-labeled-DTPA-*IRDye800*-galactosyl-dextran (FL-*gal*-dextran); a high scaled dose of FL-tilmanocept; or a co-injection of FL-tilmanocept and 5.0 nmol/g tilmanocept.

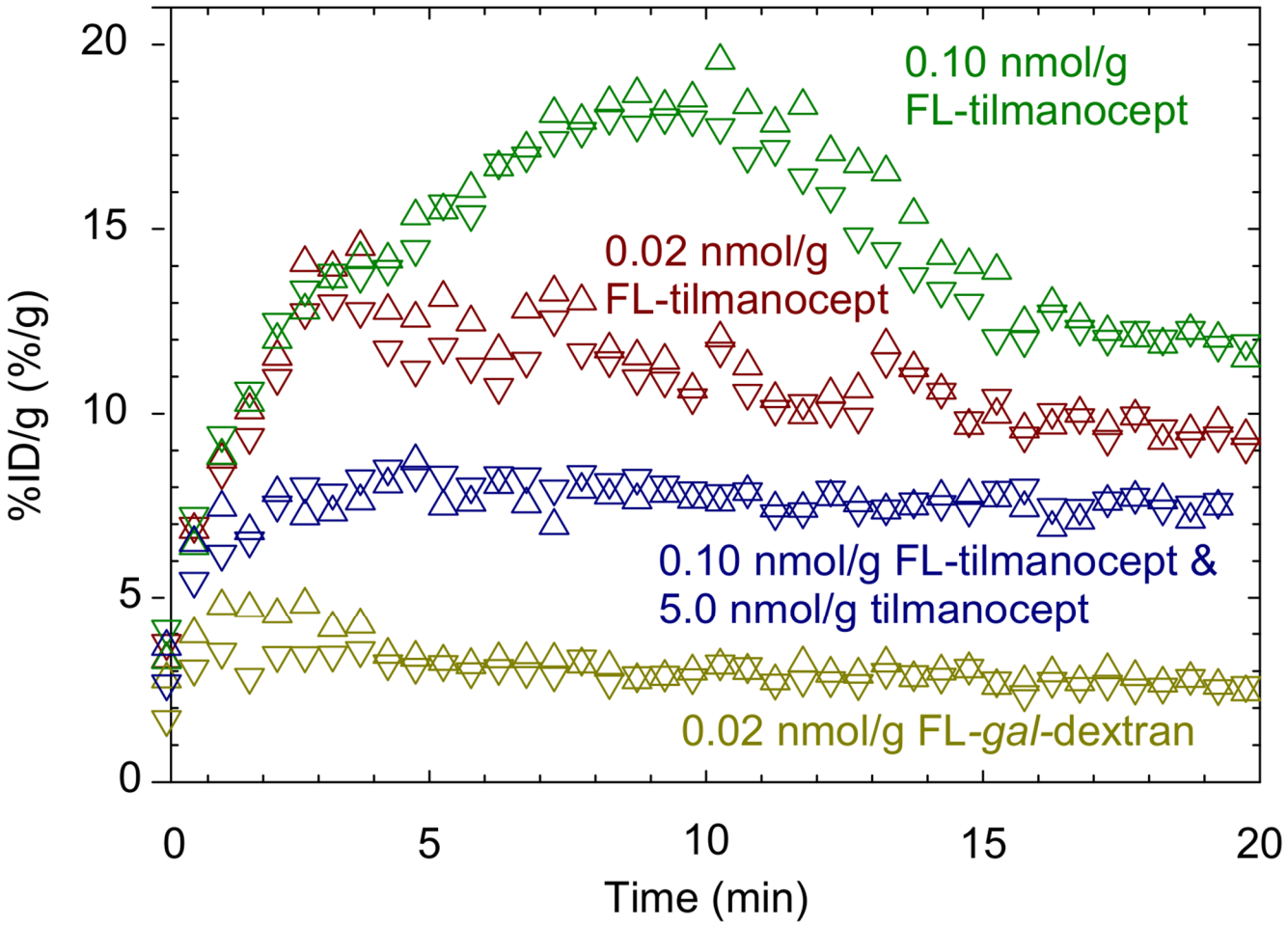

Figure 3: Renal cortex time-activity curves demonstrated receptor-mediated accumulation of tilmanocept. Left (upper triangles) and right kidney (lower triangles) time-activity curves displayed significantly different shapes after administration of: a low scaled molar dose of ^{68}Ga-labeled-*IRDye800*-tilmanocept (FL-tilmanocept) or ^{68}Ga-labeled-DTPA-*IRDye800*-galactosyl-dextran (FL-*gal*-dextran); a high scaled dose of FL-tilmanocept; or a co-injection of FL-tilmanocept and 5.0 nmol/g tilmanocept.

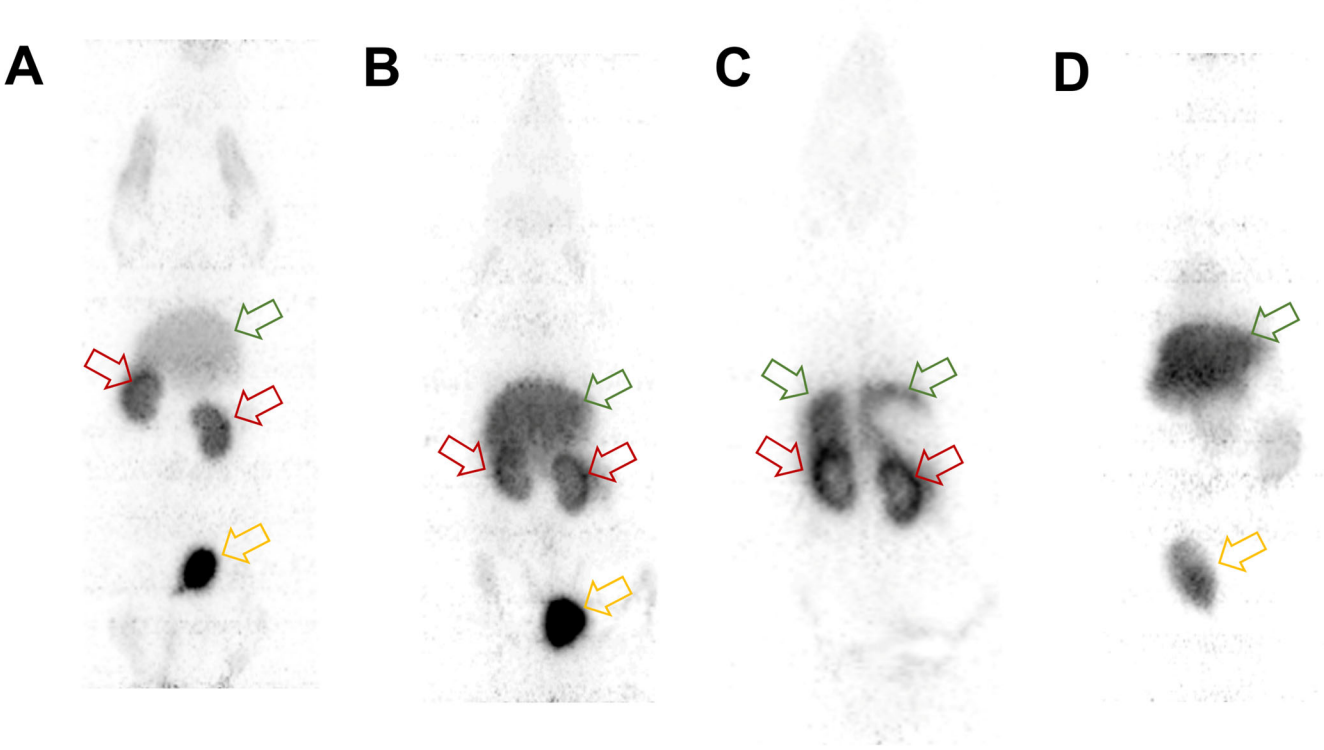

Figure 4: PET images demonstrated receptor-mediated accumulation of ^{68}Ga-*IRDye800*-tilmanocept in the renal cortex (red arrows). **(A)** A scaled high molar dose study demonstrated low liver accumulation (green arrow) compared to the kidneys, and urinary bladder (yellow arrow). **(B)** A low molar dose study demonstrated a higher liver accumulation and lower kidney accumulation. **(C)** coronal cross-sections more clearly delineates activity in the renal cortex. **(D)** A negative control study (MIP) exhibited significantly less radioactivity in the kidneys. All images were acquired 20 – 40 min PI.

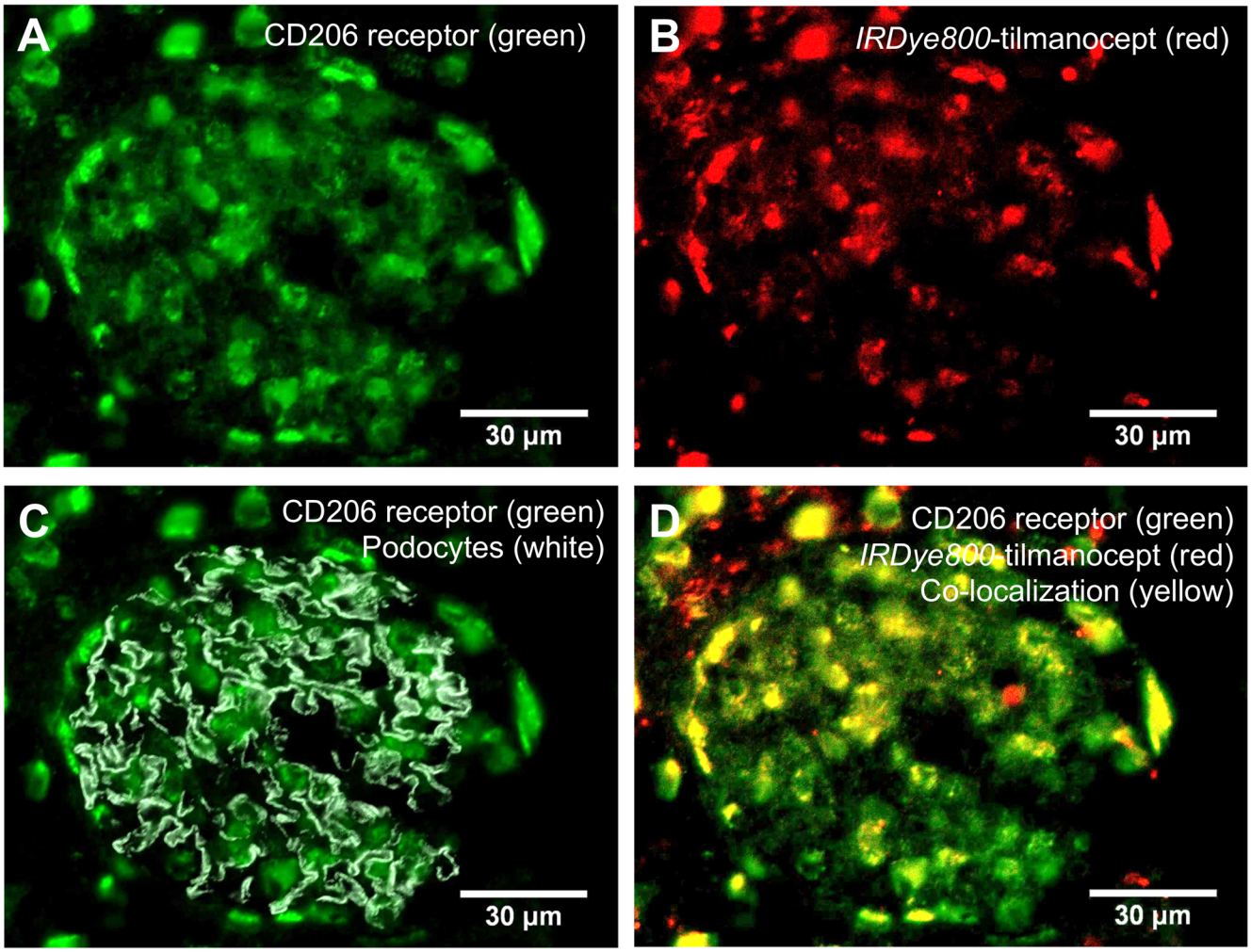

Figure 5. Histologic demonstration of tilmanocept binding to the CD206 receptor within the mesangium. Four histomicrographs from the same section of a healthy rat kidney excised 40 minutes after injection of *IRDye800CW*-tilmanocept. **(A)** A single channel representing the distribution of CD206. **(B)** A single channel representing the distribution of *IRDye800*-tilmanocept. **(C)** A two-channel composite, which demonstrates the CD206 (green) distribution within the glomerular compartment, which is defined by podocytes (grey). **(D)** A two-channel composite of the CD206 (green) and *IRDye800*-tilmanocept (red) distributions (overlapping stains result in yellow).

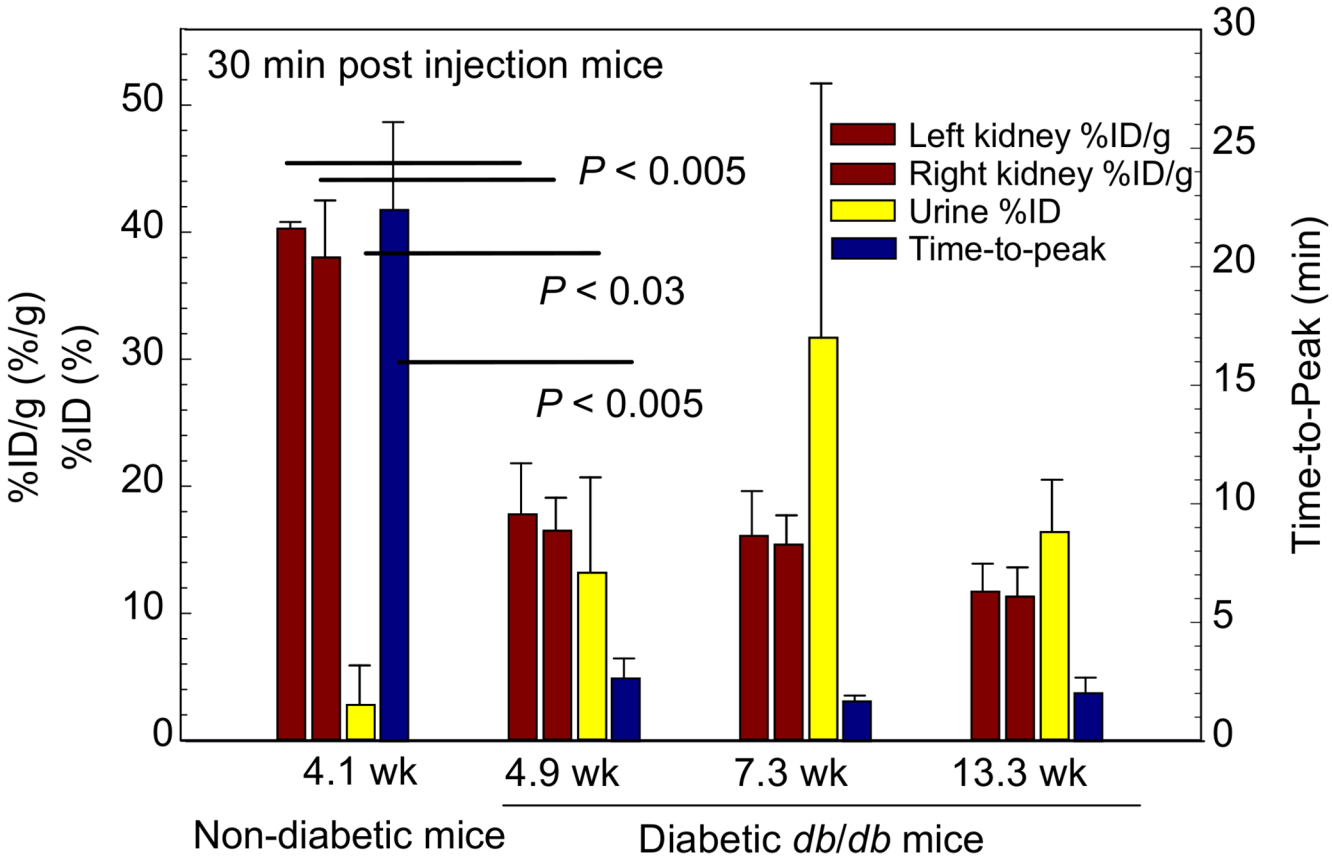

Figure 6. Studies in non-diabetic and diabetic mice demonstrated sensitivity to renal disease. The non-diabetic mice exhibited higher kidney %ID/g (red bars) and lower urine %ID than diabetic mice at 4.9, 7.3, and 13.3 weeks of age. The time-activity curves of the non-diabetic mice peaked (blue bars) later than the diabetic mice.

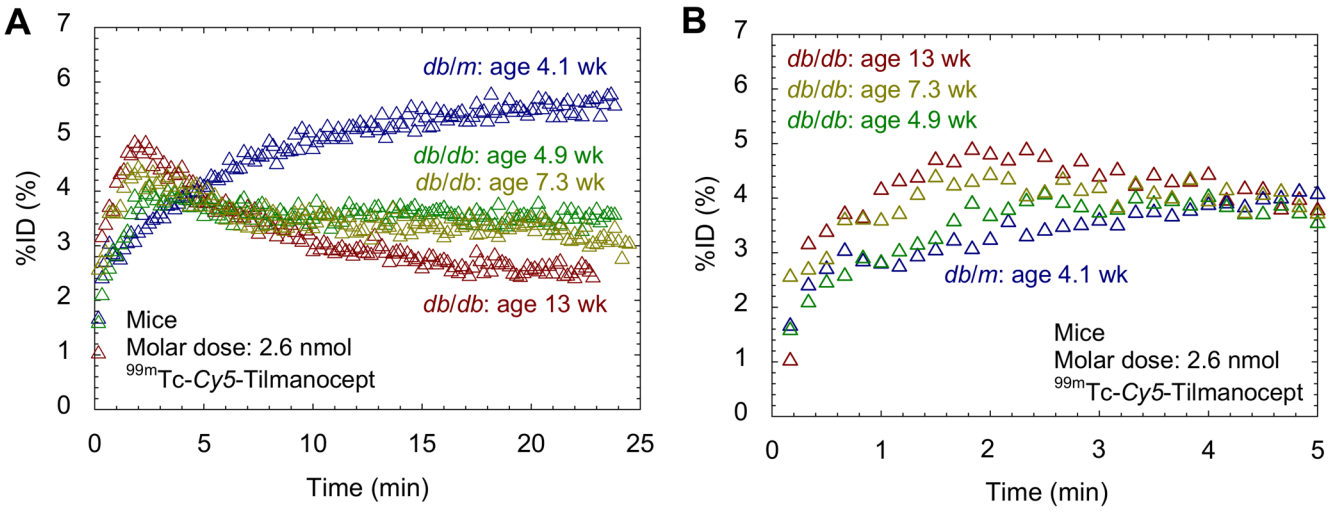

Figure 7. ^{99m}Tc-labeled tilmanocept time-activity curves **(A)** exhibited kinetic sensitivity of to chronic kidney disease. Diabetic *db*/*db* mice (green, 4.9 wk; yellow, 7.3 wk; red, 13.3 wk) exhibited peaked within 2 minutes post-injection. The non-diabetic *db*/*m* mouse (blue diamonds) peaked 18 minutes after injection. **(B)** Expanded view shows progressively faster accumulation with increasing age.

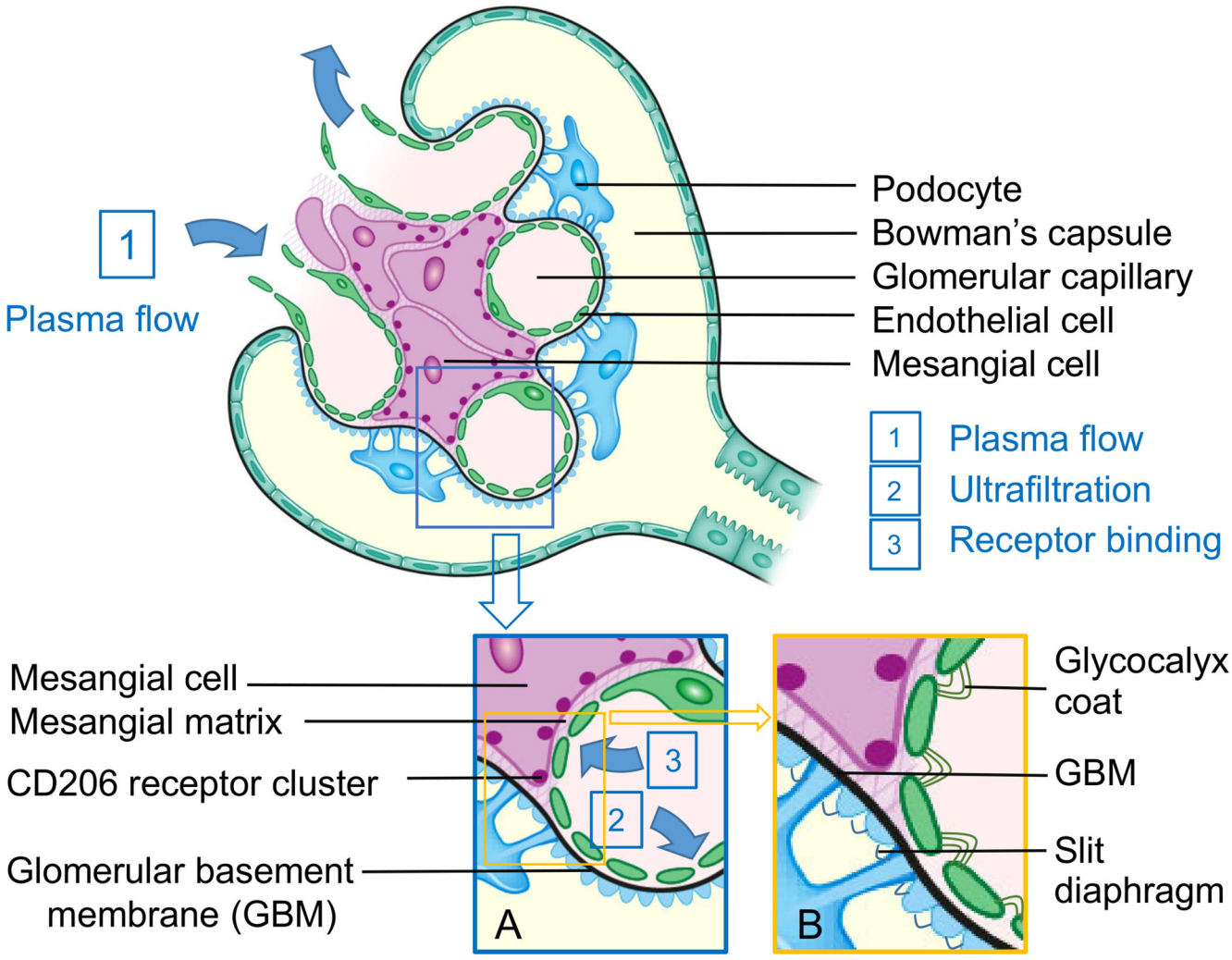

Figure 8: After delivery to the capillary lumen by renal plasma flow (Arrow 1), a molecule of radio-labeled *IRDye800*-tilmanocept can: 1) exit the glomerulus via renal plasma flow, 2) passively be ultra-filtered (Inset B, Arrow 2) into the Bowman's capsule, or 3) transverse (Inset A, Arrow 3) the mesangial cell matrix and bind to a CD206 receptor.

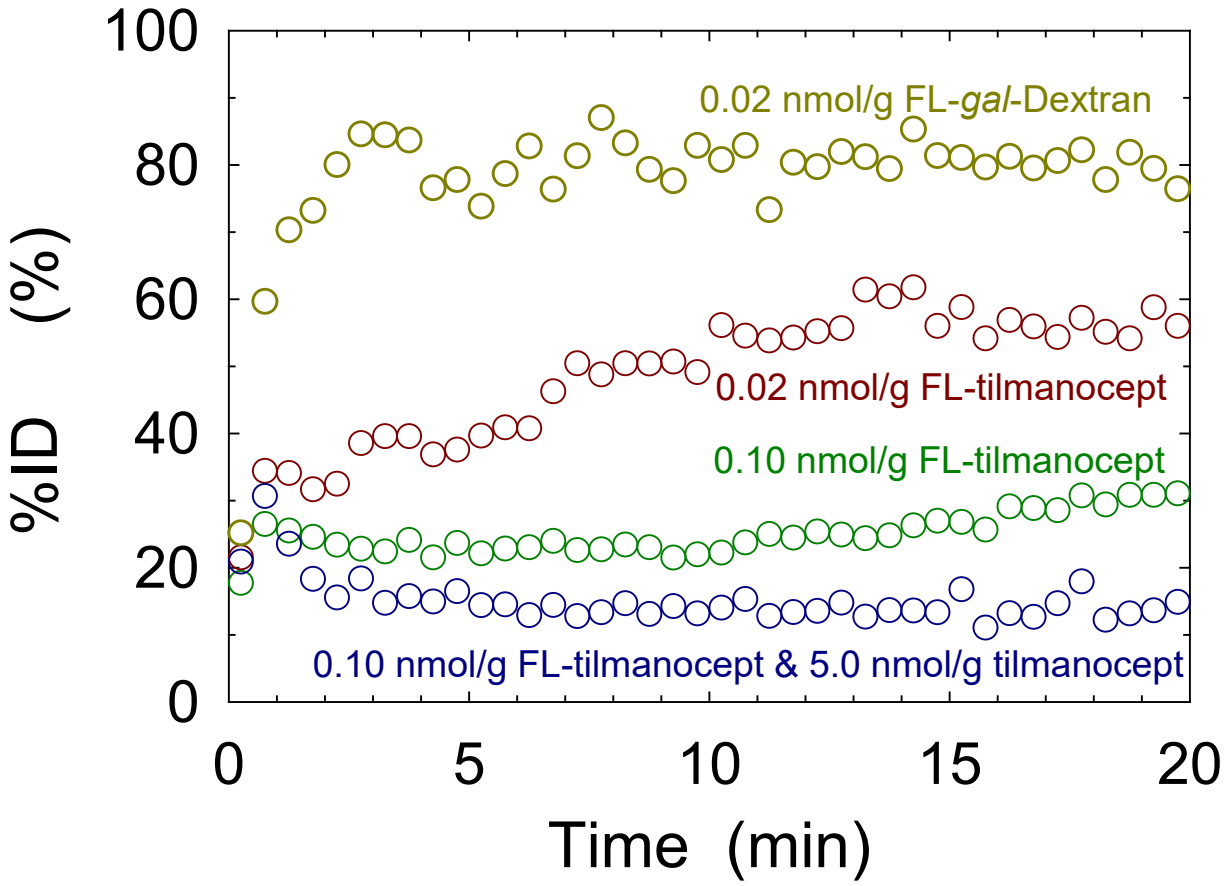

Supplemental Figure 1: Liver time-activity curves demonstrated receptor-mediated accumulation of Ga-68-labeled *IRDye800*-tilmanocept, which influenced tilmanocept uptake by the renal cortex. low (0.02 nmol/g) scaled molar dose of ^{68}Ga-labeled-*IRDye800*-tilmanocept (FL-tilmanocept) or ^{68}Ga-labeled-DTPA-*IRDye800*-galactosyl-dextran (FL-*gal*-dextran), or a high (0.10 nmol/g) scaled dose of FL-tilmanocept, or a coinjection of FL-tilmanocept and 5.0 nmol/g tilmanocept.

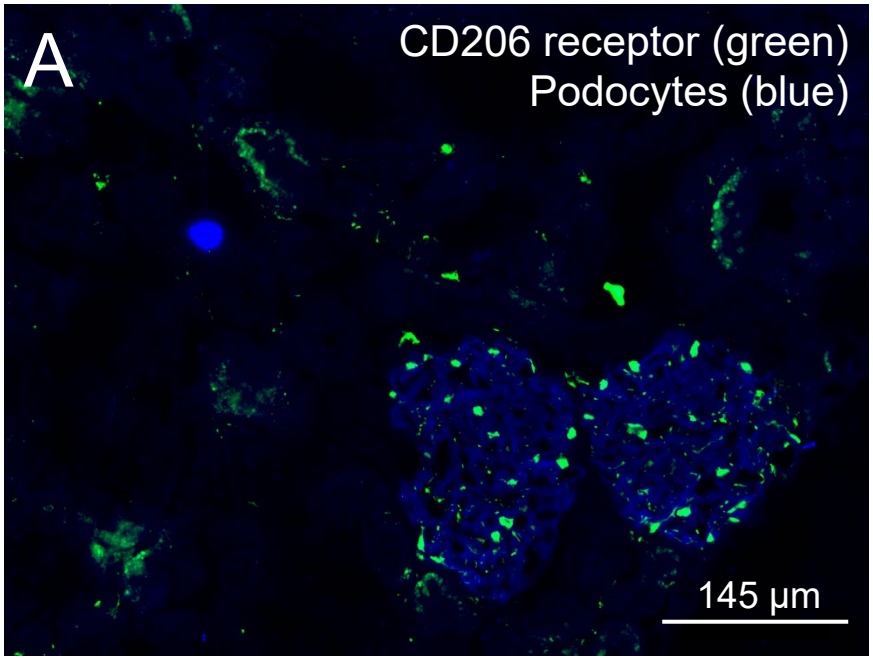

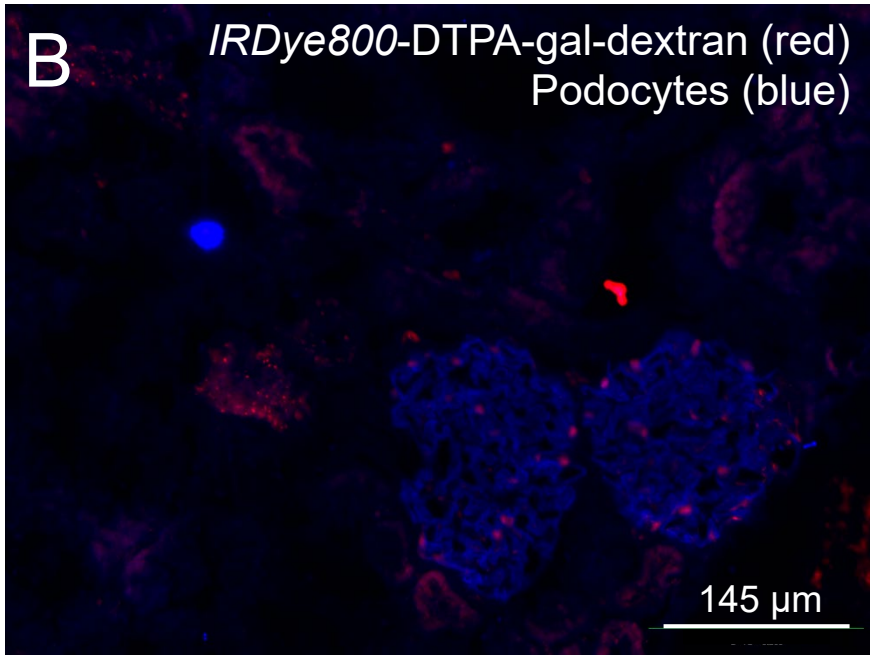

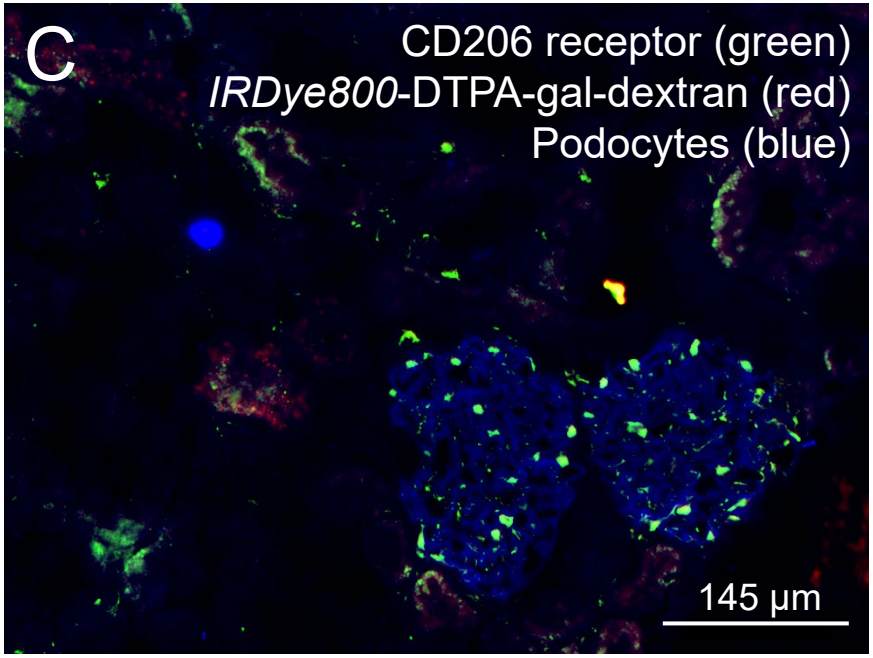

Supplemental Figure 2A. Histologic demonstration of tilmanocept specificity for the CD206 receptor. Three histomicrographs from the same section (frozen section, 5 um) of a healthy rat kidney excised 40 minutes after a 0.02-nmol/g injection of *IRDye800CW*-DTPA-galactosyl-dextran radiolabeled with gallium-68. **(A)** A dual-channel composite (*AlexaFluor488*, *AlexaFluor647*) at 20x magnification representing the distribution of podocytes (blue) and CD206 (green). **(B)** A dual-channel composite (*AlexaFluor488*, *IRDye800CW*, 20x) demonstrating the distribution of podocytes (blue) and the very low presence of *IRDye800*-DTPA-galactosyl-dextran (red). **(C)** A three-channel composite (*AlexaFluor488*, *AlexaFluor647, IRDye800CW,* 20x), which demonstrates the lack co-localization (yellow) of *IRDye800*-DTPA-galactosyl-dextran (red) and CD206 (green) within the glomerular compartment (blue).

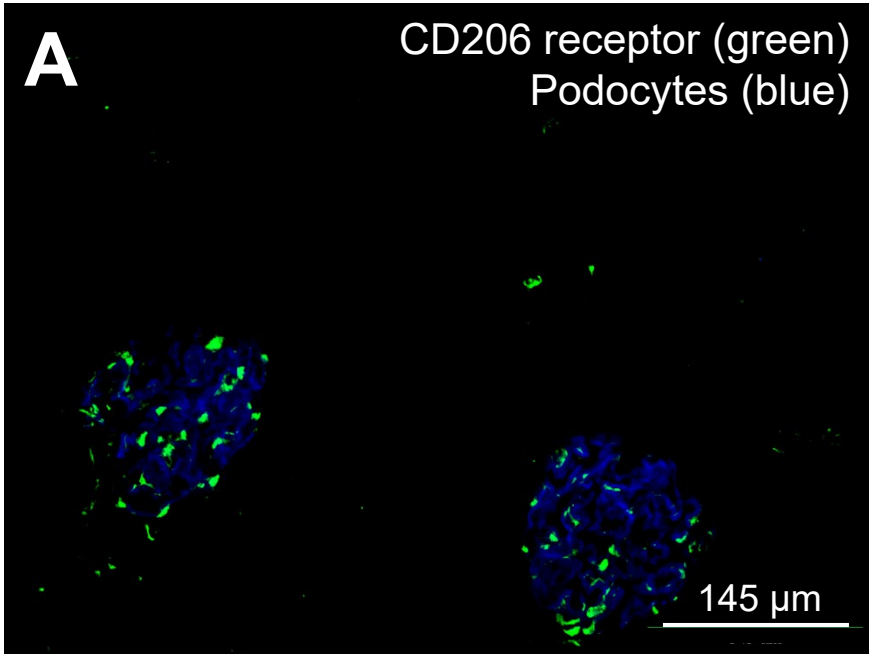

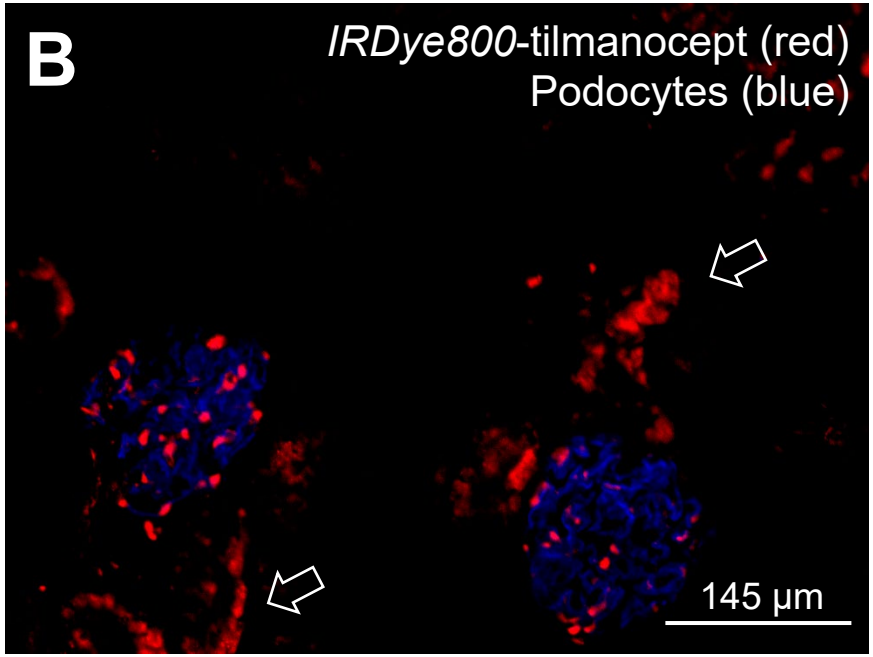

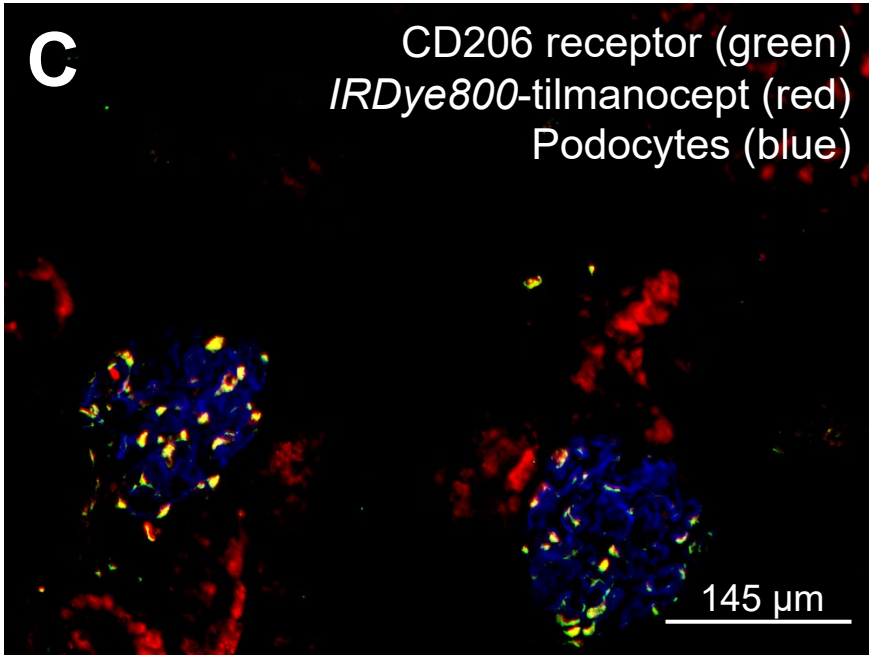

Supplemental Figure 3A. Histologic demonstration of tilmanocept binding to the CD206 receptor within the mesangium. Three histomicrographs from the same section (frozen section, 5 um) of a healthy rat kidney excised 40 minutes after a 0.1 nmol/g injection of *IRDye800*-tilmanocept radiolabeled with gallium-68. **(A)** A dual-channel composite (*AlexaFluor488*, *AlexaFluor647*) at 20x magnification representing the distribution of podocytes (blue) and CD206 (green). **(B)** A dual-channel composite (*AlexaFluor488*, *IRDye800CW*, 20x) representing the distribution of podocytes (blue) and tilmanocept (red). The presence of *IRDye800* (red) outside (arrows) of the podocyte (blue) fields is consistent with filtered *IRDye800*-tilmanocept within the renal tubules; the urinary bladder of this rat accumulated 14% of the dose during the 40-minute imaging study. **(C) A** three- channel composite (*AlexaFluor488*, *AlexaFluor647, IRDye800CW,* 20x), which demonstrates co-localization (overlapping stains result in yellow) of tilmanocept (red) and CD206 (green) within the glomerular compartment (blue).